

¹ **Pattern-based downscaling of snowpack variability in
2 the western United States**

³ Nicolas Gauthier · Kevin J. Anchukaitis ·
⁴ Bethany Coulthard

⁵
⁶ Received: date / Accepted: date

⁷ **Abstract** The decline in snowpack across the western United States is one of
8 the most pressing threats posed by climate change to regional economies and
9 livelihoods. Earth system models are important tools for exploring historical
10 and future snowpack dynamics, yet their coarse spatial resolutions distort lo-
11 cal topography and bias spatial patterns of accumulation and ablation. Here,
12 we explore pattern-based statistical downscaling for spatially-continuous in-
13 terannual snowpack variability. We find that a few leading patterns capture
14 the majority of snowpack variability across the western US in observations,
15 reanalyses, and free-running simulations. Pattern-based downscaling methods
16 yield accurate, high resolution maps that correct mean and variance biases
17 in domain-wide simulated snowpack. Methods that use large-scale patterns as
18 both predictors and predictands perform better than those that do not, but all
19 are superior to an interpolation-based “delta change” approach. These findings
20 suggest that pattern-based methods are appropriate for downscaling interan-
21 nual snowpack variability and using physically meaningful large-scale patterns
22 is more important than the details of any particular downscaling method.

²³ **Keywords** snow water equivalent · empirical orthogonal functions · canonical
24 correlation analysis · teleconnections · water resources

This research was supported by the National Science Foundation Paleo Perspectives on Climate Change (P2C2) grant AGS-1803995.

N. Gauthier
School of Geography, Development & Environment and Laboratory of Tree-Ring Research,
University of Arizona, Tucson, AZ E-mail: ngauthier@arizona.edu

K. J. Anchukaitis
School of Geography, Development & Environment and Laboratory of Tree-Ring Research,
University of Arizona, Tucson, AZ

B. Coulthard
Department of Geoscience, University of Nevada Las Vegas, Las Vegas, NV

25 1 Introduction

26 The decline in snowpack across the western United States is one of the most
27 pressing threats posed by climate change to regional economies and liveli-
28 hoods (Mankin and Diffenbaugh, 2015; Mote et al, 2018; Xiao et al, 2018;
29 Huning and AghaKouchak, 2020). Spring snowmelt is critical for regional wa-
30 ter managers—more than half of annual runoff in the western US derives from
31 snowpack (Li et al, 2017). Snow plays a central role in local and regional
32 climates and ecosystems, from its cooling effect on temperatures to its mod-
33 ulation of the timing and intensity of streamflow and soil moisture anomalies
34 (Walsh et al, 1982; Marks and Dozier, 1992; Bales et al, 2006; Maurer and
35 Bowling, 2014; Li et al, 2017). The observed decline in snowpack is the result
36 of several interacting factors including shifts in the timing and intensity of sea-
37 sonal precipitation and temperature patterns, each of which are exacerbated
38 by warming temperature trends and the attendant changes in accumulation
39 and ablation (Pierce et al, 2008; Kapnick and Hall, 2012; Pederson et al, 2013;
40 Klos et al, 2014; Xiao et al, 2018). These snowpack deficits are of a magnitude
41 and extent unprecedented in the observational period (McCabe and Wolock,
42 2009; Mote et al, 2018; Schoenemann et al, 2020) and are expected to worsen
43 in the future (Fyfe et al, 2017; Marshall et al, 2019; Siler et al, 2019).

44 Despite its importance, however, it remains difficult to observe snowpack
45 uniformly across large spatial domains. Spatially-continuous high-resolution
46 maps of snowpack are therefore a challenge to produce, particularly in areas
47 with complex terrain (Erickson et al, 2005; Meromy et al, 2013). Different
48 sensor types and measurement strategies focus on distinct—if related—facets
49 of the system, such as snow water equivalent (SWE), snow-covered area, and
50 snow depth. Each has unique uncertainties, coverage, and observational spans,
51 making them a challenge to integrate (Dozier et al, 2016; Dong, 2018). In most
52 locations the observational record only extends for a few decades into the past
53 (e.g. Serreze et al, 1999), making it difficult to place observed variability in a
54 long-term context.

55 An array of modeling approaches provide ways to estimate gaps in the
56 observational record and produce continuous spatiotemporal data products.
57 From standalone hydrological bucket models to the complex land-surface com-
58 ponents of Earth System Models, snowpack simulations attempt to capture the
59 interacting drivers of snowpack variability across spatial and temporal scales.
60 These models allow for assessments of the mechanistic uncertainty of these
61 drivers and uncertainty in their observation (Clark et al, 2011). Even simple
62 models provide useful information for constraining noisy observations (Brox-
63 ton et al, 2016a). Although the skill of current-generation snow models is high
64 overall, issues remain in the representation of processes like ablation at near-
65 freezing temperatures (Rutter et al, 2009; Broxton et al, 2016b; Krinner et al,
66 2018). Regional and global snow models must run on daily to sub-daily time
67 scales, so a reduction in spatial resolution may be required to minimize com-
68 putational costs. This tradeoff makes accurate spatial modeling of snowpack
69 difficult, even when the underlying process models are physically appropriate.

70 Snow accumulation and ablation is sensitive to local topography, particularly
71 in the mountainous regions that receive the most snowfall (Anderson
72 et al, 2014; Tennant et al, 2017; Jennings and Molotch, 2019). The resolution
73 of most simulations smooth this topography, eliminating mountain peaks and
74 introducing temperature biases that prevent snow from accumulating where
75 it otherwise would (Rhoades et al, 2018). The tendency for snow models to
76 underpredict accumulated SWE has been well documented. Xu et al (2019)
77 showed that increasing model resolution from 0.44° to 0.11° increases the accu-
78 racy of simulated SWE by 35%. Such low-snow biases in regional and global
79 snow simulations preclude their use by local water managers without correc-
80 tions to this fundamental scale mismatch. Some form of downscaling is required
81 to estimate fine-resolution snowpack maps from coarser-resolution simulation
82 outputs (McGinnis, 1997; Pons et al, 2010; Tryhorn and Degaetano, 2013).
83 However, this is increasingly accomplished via an additional high-resolution
84 regional climate model or by forcing a hydrological model with atmospheric
85 forcing data downscaled by constructed analogue methods, both of which re-
86 quire data on hourly to daily time scales, making them computationally in-
87 feasible for assessing variability on time horizons greater than a few decades
88 (Rhoades et al, 2018; Chegwidden et al, 2019; Fiddes et al, 2019).

89 Non-local “pattern-based” statistical downscaling methods are an effective
90 alternative to quickly generate fine-scale, long-term ensembles from existing
91 coarse-resolution climate model simulations. Pattern-based methods decom-
92 pose observed and simulated climate fields into a limited number of spa-
93 tiotemporal patterns or “modes of variability,” finding statistical relationships
94 that translate one set of modes into the other (Bretherton et al, 1992; Tip-
95 ppett et al, 2008; Simon et al, 2013; Maraun and Widmann, 2018). Because
96 they find associations between internally-consistent predictor and predictand
97 fields, pattern-based statistical methods share some benefits with more compu-
98 tationally expensive dynamic downscaling methods that preserve the physical
99 consistency of the simulated climate fields. These methods are “non-local” in
100 that they focus on associations between large-scale patterns, rather than local
101 associations between an observed location and the overlapping simulation grid
102 cell. The simulation grid cell that best captures the observed variability at
103 a given location is often *not* the corresponding local grid cell (van den Dool
104 et al, 2000; Maraun and Widmann, 2015; Nicholson et al, 2019). While local
105 mean conditions reflect local terrain, year-to-year departures from the mean
106 often reflect teleconnections to remote, large-scale atmosphere-ocean variabil-
107 ity (van den Dool et al, 2000; Hewitt et al, 2018). Anchoring the downscaling
108 process in these large-scale physical mechanisms leads to a higher signal to
109 noise ratio (Benestad et al, 2015), ensuring the estimated statistical relation-
110 ships are internally consistent and likely to remain stable over time.

111 Here, we explore pattern-based statistical methods for downscaling inter-
112 annual variability in March mean SWE across the western United States.
113 We find that a few leading modes—present in observations, simulations, and
114 reanalyses—capture the majority of snowpack variability in this domain. We
115 compare several related regression methods for finding associations between

observed and simulated patterns and show that even simple linear models perform well under cross validation. These methods yield accurate high resolution maps that correct mean and variance biases in domain-wide simulated SWE. Methods that use large-scale patterns as both predictors and predictands perform better than those that use those patterns on only one side of the regression equation, and all pattern-based methods are superior to a local “delta change” approach. These findings suggest that pattern-based methods are indeed appropriate for downscaling interannual snowpack variability, and that employing physically-meaningful large-scale patterns is more important for accuracy than the details of any particular downscaling method. Our findings here demonstrate the utility of applying these approaches where more computational- or data-intensive methods are impractical.

2 Data

2.1 Observations

We focus on a domain between 125°W–102°W and 31°N–49°N, covering the western US states of Arizona, California, Colorado, Idaho, Montana, Nevada, New Mexico, Oregon, Utah, Washington, and Wyoming. Observed March SWE was calculated from the University of Arizona (UA) Daily 4km SWE data product, a gridded record of daily SWE and snow depth for water years 1982–2017 at 4km resolution across the conterminous US (Broxton et al., 2019). March mean SWE has been shown to approximate the more commonly used April 1st SWE measure, but is less sensitive to potential sampling variability of a single daily value (Mankin and Diffenbaugh, 2015; Ye, 2019). The UA SWE data were based on a simple ablation and accumulation model driven by gridded daily PRISM temperature and precipitation fields (Daly et al., 2008), rescaled by relative anomalies from thousands of *in situ* observations from the SNOTEL and COOP networks (Broxton et al., 2016a; Zeng et al., 2018).

2.2 Simulations

Modeled SWE for the downscaling experiments was derived from the CERA 20th century (CERA-20C) reanalysis product (Laloyaux et al., 2018). CERA-20C is a long-term reanalysis product that uses the European Centre for Medium-Range Weather Forecast (ECMWF) system spanning 1901–2010 at six-hourly temporal resolution and ~1°spatial resolution. It assimilates sea level pressure pressure and ocean temperature observations from across this period in order to avoid temporal inconsistencies from the late introduction of, for example, satellite observations. We used the mean of the 10-member ensemble for all analyses as the individual ensemble members showed few major differences. We also analyzed outputs from the CCSM4 Last Millennium simulations (Landrum et al., 2013) and the CESM Last Millennium Ensemble

(Otto-Bliesner et al, 2016), as well as their associated 20th century extensions, in order to assess modes of snowpack variability in free-running Earth system models of different native resolutions ($\sim 1^\circ$ and $\sim 2^\circ$, respectively).

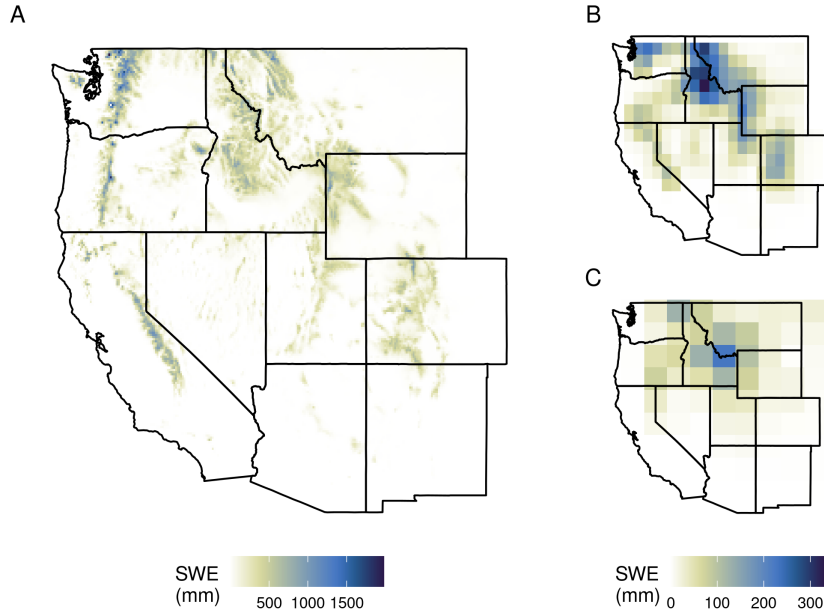


Fig. 1 Mean March snow water equivalent (SWE) in mm from A) UA 4km daily SWE observations (Broxton et al, 2019), B) CERA-20C reanalysis (Laloyaux et al, 2018), C) CESM Last Millennium Ensemble (Otto-Bliesner et al, 2016). Note the scale of the observations differs from the simulations by nearly an order of magnitude due to changes in model resolution.

158 2.3 Preprocessing

Both observed and simulated data were truncated to the overlapping period of 1982-2010 and aggregated from daily to monthly timescales by calculating the average March SWE value for each grid cell and year (Figure 1). We used bilinear interpolation to resample the large-scale simulation outputs to a common 1° grid. We also resampled the 4km snow observations to an 8km resolution to decrease computational costs without degrading the high-resolution spatial signal. Grid cells that experienced no SWE accumulation throughout the observational period were masked from successive analyses.

167 **3 Methods**

168 **3.1 Estimating modes of snowpack variability**

169 We isolated key modes of observed snowpack variability using principal com-
170 ponents analysis (PCA). The observed and simulated data were area weighted
171 by multiplying the observations at each grid cell by the square root of the cosine
172 of the cell's latitude in radians to prevent undue influence from grid
173 cells at higher latitudes (Livezey and Smith, 1999). We calculated interannual
174 SWE anomalies by mean-centering the data before analysis. We do not use
175 standardized or detrended anomalies in order to preserve spatial patterns of
176 variance across the field (Zeng et al, 2018).

177 The PCA results in a set of orthogonal principal component time series
178 or “amplitudes,” eigenvalues representing the variation accounted for by each
179 amplitude series, and eigenvectors or “empirical orthogonal functions” (EOFs)
180 mapping the amplitude time series back onto the original spatial grid. We stan-
181 dardized the PC amplitudes to unit variance and reweighted the eigenvectors
182 by the square root of their corresponding eigenvalues to give higher weight to
183 the leading spatial modes (Hannachi et al, 2007). Thus, the original dataset
184 could be reconstructed by multiplying each amplitude time series by its cor-
185 responding EOF spatial pattern, summing the results to get SWE anomalies,
186 and adding in the sample mean of the grid cell. Using only a subset of these
187 spatiotemporal patterns to reconstruct the original SWE field effectively re-
188 moves “noise” associated with the higher order modes, limiting the data to a
189 subspace representing only the most important axes of variation. The truncation
190 level k for each field was selected by cross validation (see section 3.3).

191 We used several techniques to examine the leading spatiotemporal modes.
192 We visualized the EOFs modes by calculating the Pearson correlation coeffi-
193 cient between each PC amplitude time series and each grid cell's original time
194 series. We explored potential atmosphere-ocean teleconnections by calculat-
195 ing the correlation between each PC amplitude and average January-March
196 global sea surface temperatures (SSTs), 500mb geopotential heights, and re-
197 gional temperature and precipitation, assessing statistically significant corre-
198 lations using the false discovery rate (Wilks, 2006, 2016). We also applied a
199 varimax rotation to the leading PCs to examine regional response patterns
200 (Richman, 1986), although unrotated PCs were used for downscaling due to
201 their favorable statistical properties and similarity to the rotated PCs.

202 Although we attempted to find physically-meaningful patterns where they
203 were present, we did not consider the lack of physical interpretation to be a cri-
204 terion for excluding a particular mode from the downscaling model. We ensured
205 only that the retained modes *collectively* reflected large-scale atmosphere-
206 ocean variability. In other words, the choice of truncation level k and the
207 combined set of coupled patterns were more important to our downscaling
208 process than the physical interpretation of any particular mode.

209 3.2 Pattern-based downscaling

210 Pattern-based downscaling models use some combination of observed and simulated PC time series to predict one climate field from another. There are multiple statistical methods capable of doing so, many of which are variants on 211 multiple linear regression (Bretherton et al, 1992; Tippett et al, 2008). They 212 generally differ in whether they maximize explained variance in the observations 213 as opposed to the shared variance between observations and simulations, 214 and whether they use PCs as predictors, predictands, or both (Table 1). We 215 compared three downscaling methods that spanned this methodological spectrum 216 along with an additional “local” null model.

Table 1 Pattern-based downscaling methods: canonical correlation analysis (CCA), empirical orthogonal teleconnections (EOT), principal components regression (PCR), and principal components regression via generalized additive models (PCR-GAM). Either the predictors (x), predictands (y), or both are subjected to PCA prefiltering prior to downscaling. Asymmetric models seek to explain variance of the predictands while symmetric models explain the shared correlation. Cross-validated performance metrics for the best-performing model of each class are the space-time root mean square error and the Pearson correlation between observed and simulated domain-wide SWE.

Method	PCA Prefiltering	Symmetric	RMSE	Correlation
CCA	x, y	yes	41.7	0.932
EOT	y	no	48.5	0.896
PCR	x, y	no	65.4	0.931
PCR-GAM	x, y	no	65.5	0.915

219 Canonical correlation analysis (CCA) is one of the most common approaches to coupled pattern analysis (Maraun and Widmann, 2018). It yields 220 a set of patterns that maximizes the shared correlation between the predictor 221 and predictand fields (Tippett et al, 2008). We applied CCA to the leading 222 predictor and predictand modes of variability to regularize the model and 223 make it computationally tractable (Barnett and Preisendorfer, 1987; Bretherton 224 et al, 1992; Benestad, 2001; Tippett et al, 2008). Downscaling models are 225 prone to overfitting on shorter calibration windows, so this PCA prefiltering 226 step increases the signal-to-noise ratio to ensure the resulting patterns are 227 statistically robust.

228 Principal components regression (PCR) is a similar method that uses the 229 PC time series in independent multiple linear regressions. Traditional PCR fits 230 a different model to the predictor PCs for each predictand grid cell, although 231 it is more efficient to use predictand PCs directly (Benestad et al, 2015). 232 Because the PC time series are mutually uncorrelated each predictand PC 233 can be modeled independently and there is no concern of multicollinearity. 234 PCR is asymmetric in that it only explains the variance of the predictands, 235 contrary to CCA, although both methods are linear and are equivalent under 236 certain conditions (Tippett et al, 2008). We also tested a nonlinear variant of 237

238 PCR which replaces the linear models with penalized piecewise polynomials
 239 estimated in a generalized additive model (PCR-GAM).

240 Empirical orthogonal teleconnections (EOT) finds a set of grid cells that
 241 explain the most variance in the observation domain by fitting a linear model
 242 between all pairs of predictor and predictand grid cells (van den Dool et al,
 243 2000; Appelhans et al, 2015). The simulation grid cell that predicts the most
 244 variance in all of the predictand grid cells is selected as the first pattern. Then
 245 the algorithm is run again on the residuals from the regressions on the first
 246 pattern, and the process is repeated until a set number of patterns is reached.
 247 EOT yields more localized spatial patterns, similar to rotated EOFs, than
 248 methods that use predictor and predictand PCs directly. Although PCA can
 249 be used to denoise both fields prior to the analysis, EOT focuses on the grid-
 250 cell level time series and is not constrained to fit the large scale patterns used
 251 by CCA and PCR.

252 We compared these non-local pattern-based techniques to a simple null
 253 model using interpolated simulation anomalies. This “delta change” model in-
 254 volved calculating the yearly changes in simulated SWE relative to its mean,
 255 bilinearly interpolating the low-resolution simulated multiplicative anomalies
 256 to the high resolution of the observations, and multiplying the interpolated
 257 anomalies by the high resolution observed mean. While conceptually similar to
 258 the pattern-based methods, the delta change approach uses only local informa-
 259 tion and cannot correct any spatial biases caused by the smoothed topography
 260 of the simulation. We used this model to assess and quantify the added value
 261 of the non-local downscaling approaches relative to analogous local methods.

262 All downscaling methods were implemented in R using the packages `raster`,
 263 `tidyverse`, `mgcv`, `remote`, and `MuMIN` (Wood, 2006; Appelhans et al, 2015;
 264 Wickham et al, 2019; Bartoní, 2020; Hijmans, 2020). Code for reproducing the
 265 main analysis and figures is available at <https://github.com/nick-gauthier/tidyEOF>.

266 3.3 Cross Validation

267 Each of the pattern-based downscaling methods required the number of cou-
 268 pled patterns to be defined as a hyperparameter k . The methods that used
 269 PCA prefiltering also required selection of a truncation level for the predictor
 270 and predictand PCs. We used a five-fold cross validation routine to tune the
 271 hyperparameters of each model, fitting and predicting from models with all
 272 possible combinations of up to ten predictor patterns k_x , predictand patterns
 273 k_y , and coupled patterns k_{xy} , with the constraint that $k_{xy} \leq \min(k_x, k_y)$.

274 We divided the 29-year calibration period into five contiguous folds, four of
 275 which contained six years and one of which contained five. We held out one fold
 276 at a time, fitting each model and parameter combination on the remaining folds
 277 and using them to predict the held out fold. The entire modeling workflow—
 278 anomaly calculation, PCA truncation, and model fitting—was repeated for
 279 each training and testing fold independently to prevent leaking information
 280 among the folds (Van Den Dool, 1987; Livezey and Smith, 1999; Smerdon

et al, 2010). We repeated this process until each fold had been used four times for training and once for testing, after which we combined the test folds into a single 29 year sequence from which we calculated the prediction error against the observed sequence. It is often preferable to use a nested cross validation routine when doing model selection and performance assessment simultaneously, but we did not do so in this case because our sample size was limited and the different models were of broadly the same type with a low number of similar hyperparameters (Wainer and Cawley, 2018).

We used two metrics to assess the skill of each model and parameter combination. First we examined the correlation between the observed and predicted domain-wide total SWE time series. We calculated total domain SWE by multiplying each SWE value by the area of its grid cell and summing the result. We then assessed the local spatial skill of the downscaled product by calculating the total space-time root mean square error (RMSE) between all observed and predicted grid cells. We selected the model and parameter combination that maximized domain-wide correlation and minimized RMSE under cross validation, and refit the best performing model to the entire data series. We compared the predictions from this final model to the raw CERA-20C reanalysis to assess the added value of downscaling for correcting mean and variance biases in domain-wide SWE. We also demonstrated the spatial skill of the model by comparing the spatial anomalies of observed, reanalysis, and downscaled fields during a known extreme year.

A downscaling model trained only on reanalysis data must be able to make predictions from unseen, free-running simulations to make skillful climate-change impact assessments beyond the observational period (Maraun and Widmann, 2018). As a proof-of-concept of the generalizability of the final model, we used it to downscale additional 300-year simulated snowpack sequences by projecting data from the CCSM4 and CESM Last Millennium simulations onto the reanalysis PC patterns. Here, the added value could only be assessed on a 50-year distributional basis because the free-running simulations, unlike the reanalysis, were not constrained to match the year-to-year evolution of the observations.

4 Results

A limited set of climate modes explain the majority of observed and simulated March SWE variance. Four spatiotemporal patterns explain 76% of the observed variance in March snowpack over the western United States (Figure 2a). The leading ten patterns explain nearly 90% of the observed variance. These patterns represent recurring modes of spatiotemporal variability and are an efficient means of capturing the high dimensional spatiotemporal snowpack field in a limited subspace of patterns.

Similar patterns are found in coarse-resolution simulations. The leading 10 PCs of the 110 year CERA-20C reanalysis explain 96% of the variance in simulated snowpack, and the leading four explain 89% of the variance (Figure 2b).

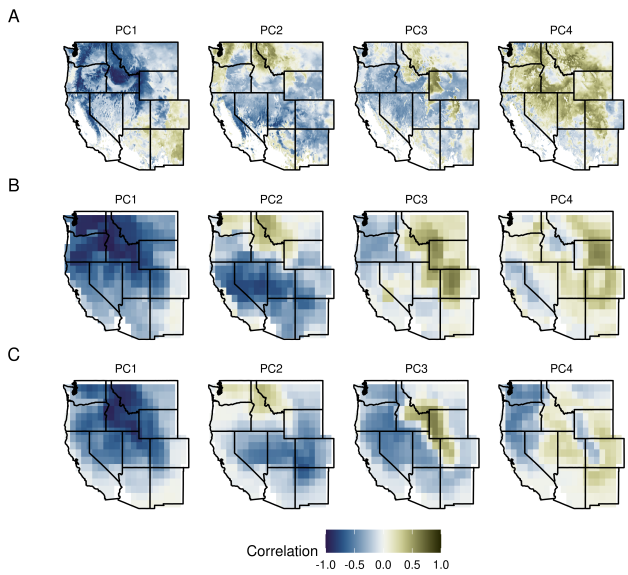


Fig. 2 The leading four EOF spatial patterns expressed as the Pearson correlation coefficient between each PC time series and March snow water equivalent in (A) UA SWE observations (1982-2017) (Broxton et al, 2019), (B) CERA-20C reanalysis (1901-1910) (Laloyaux et al, 2018), and (C) the CCSM4 Last-Millennium simulation and historical extension (850-2005) (Landrum et al, 2013). These patterns represent between 75% and 90% of the variance in their respective spatiotemporal fields.

These reanalysis PCs are associated with the same broad spatial patterns as the observed PCs, but the longer sample windows allows for greater separation between the leading modes than with the 36 year observational record.

Large-scale snow patterns reflect orography and atmosphere-ocean variability.
 The spatial EOF patterns associated with the leading snowpack PCs exhibit clear relationships to regional weather and orography as well as global sea surface temperatures and pressure systems (Figure 3). EOF/PC1 is a domain-wide signal with high loadings in the Rocky Mountains, Sierra Nevada, and Cascade ranges. It is associated with simultaneous cold and wet conditions (or vice versa) over the domain and anomalous pressure systems over northwestern North America. EOF/PC2 exhibits a north-south dipole pattern with opposite-sign loadings in the Cascades and northern Rockies and the Sierra Nevada and southern Rockies, respectively. Unlike EOF1, this pattern is associated the precipitation, not temperature, anomalies over the domain and a far more zonal geopotential height anomaly. EOF3 is localized to the Rocky Mountains and is associated with domain-wide temperature anomalies and strong SST and pressure anomalies in the north Pacific. EOF4 is a domain-wide mode associated with temperature anomalies and SST and geopotential height anomalies off the Pacific coast.

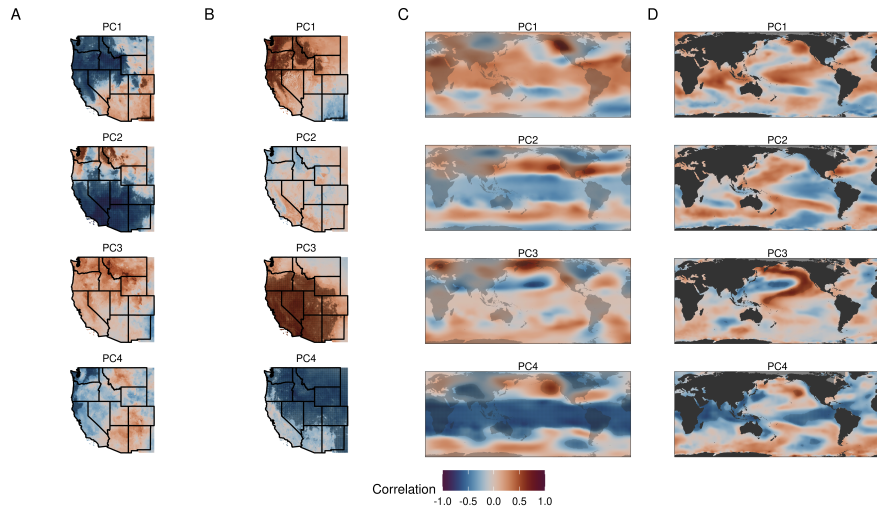


Fig. 3 Pearson correlation coefficients between the leading four observed PC time series and January–March (A) total precipitation (Daly et al, 2008), (B) average temperature (Daly et al, 2008), (C) 500mb geopotential height (Laloyaux et al, 2018), and (D) sea surface temperature (Huang et al, 2017). Stippling indicates statistically significant correlations with a false discovery rate below 0.1.

343 Higher order PCs/EOFs beyond the leading four also show spatially coherent
 344 variability, but are not interpreted here due to the orthogonality constraints
 345 and small sample size potentially leading to mixed or otherwise poorly resolved
 346 individual patterns. While many of the PC/EOF pairs are spatially coherent
 347 and may resemble physical climate patterns, the orthogonality constraints and
 348 small sample size can produce patterns spread across multiple PCs. Given the
 349 limited sample size it can be difficult to distinguish such “degenerate multiplets”
 350 from proper modes (North et al, 1982). While the first two observed PCs
 351 are distinct modes of variability, PCs 3-4 and 5-10 are degenerate multiplets
 352 that cannot be readily distinguished from one another given the limited
 353 observational period (1982-2017). Likewise, the first four reanalysis PCs
 354 represent distinct modes while PCs 5-7 and 8-10 are degenerate multiplets.
 355 A varimax rotation of the leading ten PCs alleviates some of these concerns,
 356 yielding more discrete zones reflecting topographic interception of different
 357 directions of atmospheric flow. That these patterns are present in reanalysis
 358 and simulation data from much longer time spans (1901-2010 and 840-2005,
 359 respectively) suggests the observed patterns are robust in time and can be
 360 used as anchoring points for a non-local downscaling approach.

361 *Downscaling with coupled patterns has higher cross-validated skill than similar
 362 local and non-local methods.* CCA is the best-performing downscaling model
 363 under cross validation, with the highest correlation with total western US SWE
 364 and lowest space-time root mean square error (Table 1). The most important
 365 parameter for model skill is the number of coupled patterns k_{xy} , while the

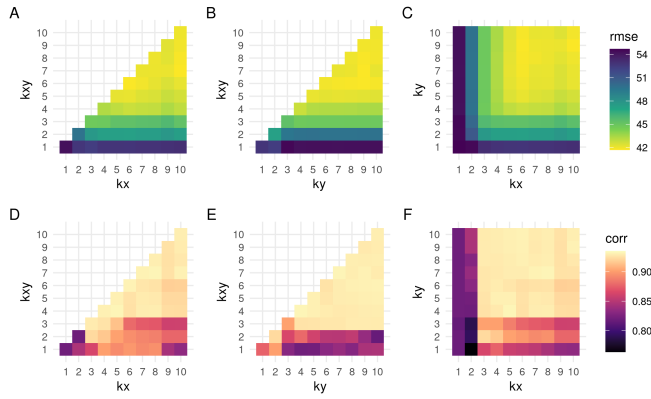


Fig. 4 Cross validation results for the three CCA parameters after Smerdon et al (2010): the number of predictor PCs k_x , the number of predictand PCs k_y , and the number of coupled patterns k_{xy} . (A)–(C) cross validation results for space-time root mean square error (lower is better). (D)–(E) correlation between observed and downscaled total domain SWE (higher is better).

366 precise number of prefiltering patterns k_x and k_y is less important as long as
 367 they are greater than or equal to the optimal number of coupled patterns (Figure
 368 4). A CCA model with four coupled patterns maximizes the domain-wide
 369 correlation, but even one coupled pattern yields a high correlation coefficient.
 370 Likewise, a model with seven coupled patterns is the most accurate in recon-
 371 structing the entire spatiotemporal field (lowest cross validated RMSE), but
 372 a four-pattern model also performs reasonably well.

373 All models have comparable skill to CCA for domain-wide SWE correla-
 374 tions, yielding a cross validated correlation of around 0.9, but there is greater
 375 spread for space-time RMSE. Both PCR models perform similarly to CCA
 376 for domain-wide SWE correlation, but the spatial skill is degraded due to the
 377 asymmetrical relationships between the predictors and predictands. PCR and
 378 PCR-GAM models produced largely similar reconstructions, as expected, but
 379 the nonlinear PCR-GAM consistently performs slightly worse than the linear
 380 PCR method due to its potential to overfit.

381 EOT yielded spatial patterns similar to the coupled-pattern methods but
 382 with notably more instability under cross validation than the pattern meth-
 383 ods because the base grid cell tended to vary between folds (Figure 5). All
 384 methods are considerably better than the delta change approach, as the use of
 385 multiplicative anomalies introduced several artifacts in areas with unusually
 386 high or low snow anomalies that significantly degraded the overall spatial skill.
 387 These results support the interpretation that anchoring downscaling relation-
 388 ships in spatial patterns, rather than grid-cell level relationships, increases the
 389 robustness of the resulting downscaled predictions.

390 *Downscaling reduces spatial and temporal biases in simulated snowpack.* Down-
 391 scaling the CERA-20C reanalysis with any of the above pattern-based methods

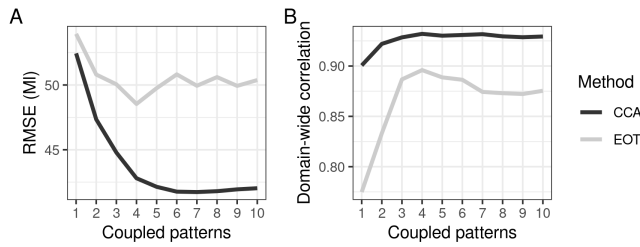


Fig. 5 Comparison of CCA and EOT downscaling under five-fold cross validation. (A) Space-time root mean square error, in megaliters of SWE, for increasing number of coupled patterns. Lower RMSE corresponds to more accurate reconstructions. (B) Correlation between observed and reconstructed total SWE over western North America. Note the performance of EOT degrades with greater than four patterns for both skill metrics because of instability in the estimated grid cell base points.

392 considerably reduces spatial and temporal biases in the raw reanalysis. With-
 393 out downscaling, the CERA-20C reanalysis tends to underpredict domain-wide
 394 total SWE averages and overpredict their variance. CCA downscaling with
 395 four coupled patterns reduces this mean and variance bias relative to obser-
 396 vations (Figure 6). By construction, pattern-based downscaling also improves
 397 the spatial structure of simulated SWE anomalies and removes spatial biases
 398 caused by the coarse resolution of the simulated topography in a way that in-
 399 terpolating the simulated anomalies does not (Figure 7). The same statistical
 400 model, fit to the reanalysis data, also reduces the spatial and temporal biases
 401 in the free-running CCSM4 Last Millennium simulation, but not the coarser
 402 CESM simulation, suggesting the model generalizes well to datasets with sim-
 403 ilar native resolution to the training set (Figure 8). Pattern-based downscaling
 404 thus provides clear added value for assessing long term patterns of change in
 405 snowpack across space and through time.

406 5 Discussion

407 A small number of climatic modes explain the majority of observed and sim-
 408 ulated interannual variance in snowpack across the western United States.
 409 Four to seven of these coupled modes are sufficient to downscale accurate
 410 high-resolution maps of regional snow water equivalent from coarse-resolution
 411 climate simulations. Even an extremely simple model with only one mode is
 412 able to reproduce the time evolution of the total volume of water stored in
 413 snow across the whole domain, although this is unlikely to be sufficient for
 414 full field spatiotemporal analyses. In spite of known biases in simulated SWE
 415 arising from issues of scale and process uncertainty, these findings suggest mod-
 416 ern numerical simulations capture enough of the large scale atmosphere-ocean
 417 dynamics that drive interannual snowpack variability and are appropriate pre-
 418 dictors for high resolution downscaling products.

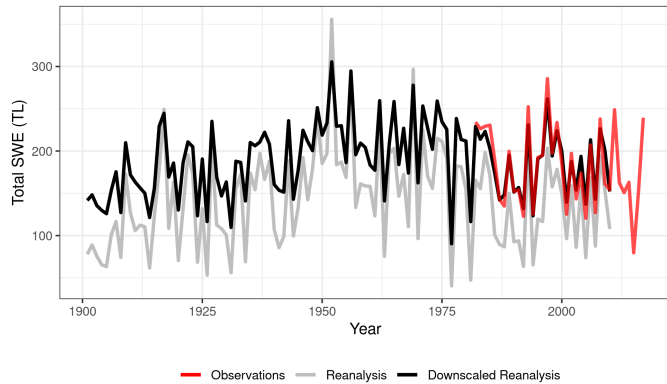


Fig. 6 Total Western US March SWE in teraliters (km^3) from the CERA-20C reanalysis with four-pattern CCA downscaling (black) and without (gray), compared to recent observations (red). Downscaling adds value to the raw reanalysis by increasing the mean and decreasing the variance relative to observations.

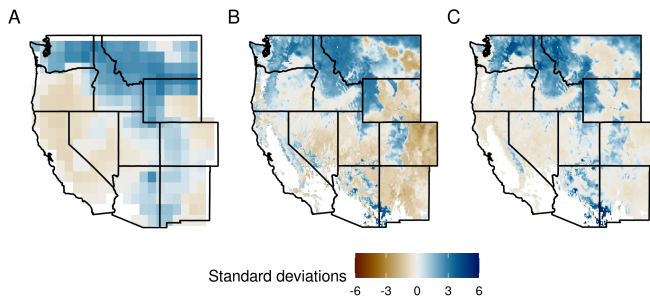


Fig. 7 Standardized SWE anomalies for the 1997 El Niño in (A) CERA-20C reanalysis, (B) downscaled CERA-20C reanalysis using CCA with seven coupled patterns, and (C) observations. Note the lower standardized anomalies in the observations relative to the downscaled reanalysis, due to residual unexplained variance in the observations.

Given judicious choice of physically meaningful patterns as predictors and predictands, even a simple linear downscaling method yields skillful hindcasts of observed SWE variability. This approach relies on the ability of climate and weather models to accurately simulate large-scale atmosphere-ocean variability. Rather than deriving complex transfer functions between a variety of local variables—a process that often breaks the physical consistency of climate model outputs—this approach uses the internal physical consistency of those simulations to its advantage by finding a simple mapping between simulated and observed dynamics. Anchoring statistical downscaling methods in a mechanistic understanding of the climate system, instead of using downscaling as a replacement for that understanding, is of paramount importance to any downscaling project.

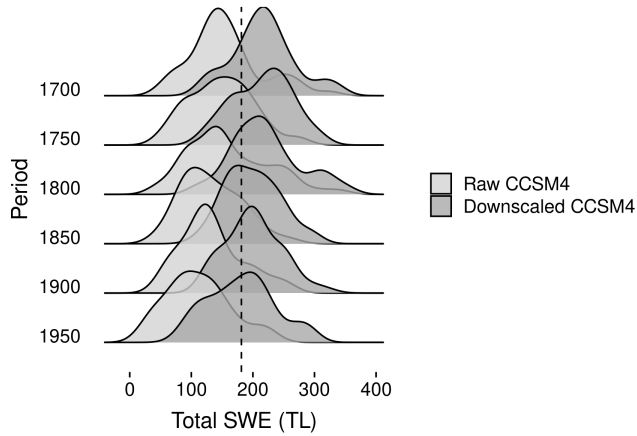


Fig. 8 Total Western US March SWE in teraliters (km^3) from the CCSM4 Last Millennium simulation (Landrum et al, 2013) with CCA downscaling (dark gray) and without (light gray), compared to the 1982-2017 observed mean (dashed line). Unlike CERA-20C, CCSM4 is not constrained to be synchronous with observations and is instead assessed on a 50-year distributional basis. The same model fit from Figure 6 is used here, with the CCSM4 data simply projected onto the reanalysis PC space to enable downscaling. This approach was less successful when applied to CESM-LME outputs (not shown), as its $\sim 2^\circ$ native resolution was too coarse to meaningfully project onto the 1° reanalysis patterns.

431 The leading two principal modes of variability highlighted in this study—a
 432 coherent domain-wide signal and a north/south dipole—have been identified
 433 previously in observational data of snow and several variables (Redmond and
 434 Koch, 1991; Cayan, 1996; McCabe and Dettinger, 2002; Jin et al, 2006; Mc-
 435 Cabe et al, 2013; Pederson et al, 2013; Malevich and Woodhouse, 2017). The
 436 first mode represents a domain-wide temperature anomaly associated with
 437 PNA-type atmospheric circulation. The second represents the influence of
 438 tropical Pacific SST variability (ENSO, PDO) deflecting storm tracks north or
 439 south and causing coincident temperature and precipitation anomalies in each
 440 region. This pair of influences is robust over time and appears in long-term
 441 tree-ring reconstructions from similar domains (Woodhouse, 2003; Pederson
 442 et al, 2011; Coulthard, 2015; Barandiaran et al, 2017).

443 There is less certainty as to the drivers of the successive modes of vari-
 444 ability. Possible influences include cold vs. warm El Niño years, atmospheric
 445 rivers, temperature anomalies due to the Northern Annular Mode and North
 446 Atlantic Oscillation, or overlapping multidecadal modes of Pacific SST vari-
 447 ability (QDO, PDO, IPO) (Ghatak et al, 2010; Seager et al, 2010; Barrett et al,
 448 2015; Barandiaran et al, 2017; Goldenson et al, 2018). Complicating matters
 449 further is that the same large scale pattern can influence snowpack through
 450 multiple physical pathways and different teleconnections can act through the
 451 same pathway (Mote, 2003; Ge et al, 2009; Ghatak et al, 2010). For exam-
 452 ple, ENSO variability influences both temperature and precipitation, and by
 453 extension snow accumulation and ablation, simultaneously. Likewise, Pacific

454 SST variability can influence storm tracks across multiple spatial and temporal
455 scales.

456 Ultimately, these large-scale patterns represent the outcome of nonlinear,
457 interacting processes that may not necessarily be well represented by linear
458 statistical methods like PCA and CCA. What may appear to be distinct cli-
459 matic modes in a PCA may instead reflect the methods' linearity assumptions
460 and orthogonality constraints. While these methods are nevertheless useful
461 for downscaling because they isolate the parsimonious subspace of variability
462 most influenced by these large-scale dynamics, interpretations of the individual
463 modes must always be treated with caution. An alternative approach would
464 be to use nonlinear feature extraction methods such as independent compo-
465 nents analysis, self-organizing maps, or autoencoders to generate statistically
466 independent patterns with increased interpretability and out-of-sample pre-
467 dictability (Reusch et al, 2005; Fassnacht and Derry, 2010; Henderson et al,
468 2017; Baño-Medina et al, 2020; He and Eastman, 2020). However, the risk
469 of overfitting nonlinear methods remains high given the short observational
470 window.

471 Regardless of whether this large-scale variability is captured by linear or
472 nonlinear methods there will always remain a degree of unexplained local vari-
473 ability. About 20% of the local SWE variance observed at the grid cell level is
474 left unexplained by the large-scale patterns. By definition, methods that used
475 a restricted number of patterns on the left hand side of the regression equation
476 will explain only a subset of the observed variance. Ideally, a downscaled SWE
477 product would preserve this full range of variability and give some insight into
478 the uncertainty in the downscaled estimates (Hewitt et al, 2018). An intuitive
479 approach would be to add the residual variance back to each grid cell as un-
480 correlated white noise. However, we find here that the residual fraction here
481 is non-normal, spatially autocorrelated, and varies in magnitude across the
482 study domain. While an analytical solution to the CCA noise fraction exists
483 (Wilks, 2014), a more pragmatic approach may be to fit Gaussian process or
484 copula models to the cross-validated errors directly. Regardless of the precise
485 method, this residual internal variability should be modeled in order to yield
486 downscaled data appropriate for localized climate-change impact assessments
487 (Towler et al, 2017).

488 The potential uses for downscaled snowpack estimates are many. However,
489 to be truly useful to researchers, stakeholders, and policy makers, downscaled
490 snowpack products should take advantage of the wide range of long-term pa-
491 leoclimatic simulations to generate long-term ensembles of fine-scale snowpack
492 variability. Future work should apply the methods explored here to the full
493 ensemble of simulations from the CMIP Last Millennium experiments (Otto-
494 Bliesner et al, 2016), providing a long-term perspective on present and future
495 changes to snowpack and a spatially-continuous baseline for use in paleocli-
496 mate data assimilation (Hakim et al, 2016; Devers et al, 2019; Fiddes et al,
497 2019; Girotto et al, 2020). Appropriate predictor patterns can be extracted us-
498 ing Common EOF analysis on combined reanalysis and GCM fields (Benestad,
499 2001), and informed by perfect model experiments to ensure that a long-term

500 climate change signal can be captured by changes in the modes themselves
501 rather than by modes lacking analogues in the present climate.

502 References

- 503 Anderson BT, McNamara JP, Marshall HP, Flores AN (2014) Insights into
504 the physical processes controlling correlations between snow distribution
505 and terrain properties. *Water Resources Research* 50:1–19, DOI 10.1002/
506 2013WR013714
- 507 Appelhans T, Detsch F, Nauss T (2015) Remote: Empirical orthogonal
508 teleconnections in R. *Journal of Statistical Software* 65(10):1–19, DOI
509 10.18637/jss.v065.i10
- 510 Bales RC, Molotch NP, Painter TH, Dettinger MD, Rice R, Dozier J (2006)
511 Mountain hydrology of the western United States. *Water Resources Re-*
512 *search* 42(8):1–13, DOI 10.1029/2005WR004387
- 513 Baño-Medina J, Manzanas R, Gutierrez JM (2020) Configuration and inter-
514 comparison of deep learning neural models for statistical downscaling. *Geo-*
515 *scientific Model Development* 13(4):2109–2124, DOI 10.5194/gmd-13-2109-
516 2020
- 517 Barandiaran D, Wang SY, De Rose RJ (2017) Gridded snow water equivalent
518 reconstruction for Utah using forest inventory and analysis tree-ring data.
519 *Water* 9(6):1–13, DOI 10.3390/w9060403
- 520 Barnett TP, Preisendorfer R (1987) Origins and Levels of Monthly and Sea-
521 sonal Forecast Skill for United States Surface Air Temperatures Determined
522 by Canonical Correlation Analysis. *Monthly Weather Review* 115(9):1825–
523 1850, DOI 10.1175/1520-0493(1987)115<1825:oaloma>2.0.co;2
- 524 Barrett BS, Henderson GR, Werling JS (2015) The Influence of the MJO on
525 the intraseasonal variability of Northern Hemisphere spring snow depth.
526 *Journal of Climate* 28(18):7250–7262, DOI 10.1175/JCLI-D-15-0092.1
- 527 Bartoń K (2020) MuMIn: Multi-model inference. R package version 1.43.17.
528 URL <https://cran.r-project.org/package=MuMIn>
- 529 Benestad RE (2001) A Comparison Between Two Empirical Downscal-
530 ing Strategies. *International Journal of Climatology* 21:1645–1668, DOI
531 10.1002/joc.703
- 532 Benestad RE, Chen D, Mezghani A, Fan L, Parding K (2015) On using
533 principal components to represent stations in empirical-statistical down-
534 scaling. *Tellus, Series A: Dynamic Meteorology and Oceanography* 6(1),
535 DOI 10.3402/tellusa.v67.28326
- 536 Bretherton CS, Smith C, Wallace JM (1992) An Intercomparison of Methods
537 for Finding Coupled Patterns in Climate Data. *Journal of Climate* 5(6):541–
538 560, DOI 10.1175/1520-0442(1992)005<0541:aiomff>2.0.co;2
- 539 Broxton PD, Dawson N, Zeng X (2016a) Linking snowfall and snow accumu-
540 lation to generate spatial maps of SWE and snow depth. *Earth and Space*
541 *Science* 3:246–256, DOI 10.1002/2016EA000174

- 542 Broxton PD, Zeng X, Dawson N (2016b) Why do global reanalyses and land
543 data assimilation products underestimate snow water equivalent. *Journal of*
544 *Hydrometeorology* 17(11):2743–2761, DOI 10.1175/JHM-D-16-0056.1
- 545 Broxton PD, Zeng X, Dawson N (2019) Daily 4 km Gridded SWE and Snow
546 Depth from Assimilated In-Situ and Modeled Data over the Conterminous
547 US, Version 1. DOI 10.5067/0GGPB220EX6A
- 548 Cayan DR (1996) Interannual climate variability and snowpack in the west-
549 ern United States. *Journal of Climate* 9(5):928–948, DOI 10.1175/1520-
550 0442(1996)009<0928:ICVASI>2.0.CO;2
- 551 Chegwidden OS, Nijssen B, Rupp DE, Arnold JR, Clark MP, Hamman JJ,
552 Kao SC, Mao Y, Mizukami N, Mote PW, Pan M, Pytlak E, Xiao M
553 (2019) How Do Modeling Decisions Affect the Spread Among Hydrologic
554 Climate Change Projections? Exploring a Large Ensemble of Simulations
555 Across a Diversity of Hydroclimates. *Earth's Future* 7(6):623–637, DOI
556 10.1029/2018EF001047
- 557 Clark MP, Hendrikx J, Slater AG, Kavetski D, Anderson B, Cullen NJ, Kerr
558 T, Örn Hreinsson E, Woods RA (2011) Representing spatial variability of
559 snow water equivalent in hydrologic and land-surface models: A review.
560 *Water Resources Research* 47(7), DOI 10.1029/2011WR010745
- 561 Coulthard B (2015) Multi-century records of snow water equivalent and
562 streamflow drought from energy-limited tree rings in south coastal British
563 Columbia. PhD thesis, University of Victoria
- 564 Daly C, Halbleib M, Smith JI, Gibson WP, Doggett MK, Taylor GH, Curtis
565 J, Pasteris PP (2008) Physiographically sensitive mapping of climatologi-
566 cal temperature and precipitation across the conterminous United States.
567 *International Journal of Climatology* 28:2031–2064, DOI 10.1002/joc.1688
- 568 Devers A, Vidal J, Lauvernet C, Graff B, Vannier O (2019) A framework for
569 high-resolution meteorological surface reanalysis through offline data assim-
570 ilation in an ensemble of downscaled reconstructions. *Quarterly Journal of*
571 *the Royal Meteorological Society* 146:153–173, DOI 10.1002/qj.3663
- 572 Dong C (2018) Remote sensing, hydrological modeling and in situ
573 observations in snow cover research: A review. *Journal of Hy-
574 drology* 561(March):573–583, DOI 10.1016/j.jhydrol.2018.04.027, URL
575 <https://doi.org/10.1016/j.jhydrol.2018.04.027>
- 576 van den Dool HM, Saha S, Johansson Å (2000) Empirical orthogonal
577 teleconnections. *Journal of Climate* 13(8):1421–1435, DOI 10.1175/1520-
578 0442(2000)013<1421:EOT>2.0.CO;2
- 579 Dozier J, Bair EH, Davis RE (2016) Estimating the spatial distribution of
580 snow water equivalent in the world’s mountains. *WIREs Water* 3(3):461–
581 474, DOI 10.1002/wat2.1140
- 582 Erickson TA, Williams MW, Winstral A (2005) Persistence of topographic
583 controls on the spatial distribution of snow in rugged mountain terrain,
584 Colorado, United States. *Water Resources Research* 41(4):1–17, DOI
585 10.1029/2003WR002973
- 586 Fassnacht SR, Derry JE (2010) Defining similar regions of snow in the Col-
587 orado River Basin using self-organizing maps. *Water Resources Research*

- 588 46(W04507), DOI 10.1029/2009WR007835
- 589 Fiddes J, Aalstad K, Westermann S (2019) Hyper-resolution ensemble-based
590 snow reanalysis in mountain regions using clustering. *Hydrology and Earth
591 System Sciences* 23(11):4717–4736, DOI 10.5194/hess-23-4717-2019
- 592 Fyfe JC, Derksen C, Mudryk L, Flato GM, Santer BD, Swart NC, Molotch
593 NP, Zhang X, Wan H, Arora VK, Scinocca J, Jiao Y (2017) Large near-term
594 projected snowpack loss over the western United States. *Nature Communica-
595 tions* 8(14996), DOI 10.1038/ncomms14996
- 596 Ge Y, Gong G, Frei A (2009) Physical mechanisms linking the winter Pacific-
597 North American teleconnection pattern to spring North American snow
598 depth. *Journal of Climate* 22(19):5135–5148, DOI 10.1175/2009JCLI2842.1
- 599 Ghatak D, Gong G, Frei A (2010) North American temperature, snowfall,
600 and snow-depth response to winter climate modes. *Journal of Climate*
601 23(9):2320–2332, DOI 10.1175/2009JCLI3050.1
- 602 Girotto M, Musselman KN, Essery RL (2020) Data Assimilation Improves Es-
603 timates of Climate-Sensitive Seasonal Snow. *Current Climate Change Re-
604 ports* 6:81–94, DOI 10.1007/s40641-020-00159-7
- 605 Goldenson N, Leung LR, Bitz CM, Blanchard-Wrigglesworth E (2018) Influ-
606 ence of atmospheric rivers on mountain snowpack in the western United
607 States. *Journal of Climate* 31(24):9921–9940, DOI 10.1175/JCLI-D-18-
608 0268.1
- 609 Hakim GJ, Emile-Geay J, Steig EJ, Noone D, Anderson DM, Tardif
610 R, Steiger N, Perkins WA (2016) The Last Millennium Climate Re-
611 analysis Project: Framework and First Results. *Journal of Geophysical
612 Research: Atmospheres* 98195:1–56, DOI 10.1002/2016JD024751, URL
613 <http://doi.wiley.com/10.1002/2016JD024751>
- 614 Hannachi A, Jolliffe IT, Stephenson DB (2007) Empirical orthogonal func-
615 tions and related techniques in atmospheric science: A review. *International
616 Journal of Climatology* 27:1119–1152, DOI 10.1002/joc.1499
- 617 He J, Eastman JR (2020) A sequential autoencoder for teleconnection analysis.
618 *Remote Sensing* 12(5):53–54, DOI 10.3390/rs12050851
- 619 Henderson GR, Barrett BS, South K (2017) Eurasian October snow water
620 equivalent: using self-organizing maps to characterize variability and identify
621 relationships to the MJO. *International Journal of Climatology* 37(2):596–
622 606, DOI 10.1002/joc.4725
- 623 Hewitt J, Hoeting JA, Done JM, Towler E (2018) Remote effects spatial pro-
624 cess models for modeling teleconnections. *Environmetrics* 29(8):1–14, DOI
625 10.1002/env.2523, 1612.06303
- 626 Hijmans RJ (2020) raster: Geographic Data Analysis and Modeling. R package
627 version 3.3-13. URL <https://cran.r-project.org/package=raster>
- 628 Huang B, Thorne PW, Banzon VF, Boyer T, Chepurin G, Lawrimore
629 JH, Menne MJ, Smith TM, Vose RS, Zhang HM (2017) NOAA Ex-
630 tended Reconstructed Sea Surface Temperature (ERSST), Version 5. DOI
631 10.7289/V5T72FNM
- 632 Huning LS, AghaKouchak A (2020) Approaching 80 years of snow water equiv-
633 alent information by merging different data streams. *Scientific Data* 7(1),

- 634 DOI 10.1038/s41597-020-00649-1
- 635 Jennings KS, Molotch NP (2019) The sensitivity of modeled snow ac-
636 cumulation and melt to precipitation phase methods across a climatic
637 gradient. *Hydrology and Earth System Sciences* 23:3765–3786, DOI
638 <https://doi.org/10.5194/hess-23-3765-2019>
- 639 Jin J, Miller NL, Sorooshian S, Gao X (2006) Relationship between atmo-
640 spheric circulation and snowpack in the western USA. *Hydrological Pro-
641 cesses* 20(4):753–767, DOI 10.1002/hyp.6126
- 642 Kapnick S, Hall A (2012) Causes of recent changes in western North American
643 snowpack. *Climate Dynamics* 38(9–10):1885–1899, DOI 10.1007/s00382-011-
644 1089-y
- 645 Klos PZ, Link TE, Abatzoglou JT (2014) Extent of the rain-snow transition
646 zone in the western U.S. under historic and projected climate. *Geophysical
647 Research Letters* 41:4560–4568, DOI 10.1002/2014GL060500
- 648 Krinner G, Derksen C, Essery R, Flanner M, Hagemann S, Clark M, Hall
649 A, Rott H, Brutel-Vuilmet C, Kim H, Ménard CB, Mudryk L, Thackeray
650 C, Wang L, Arduini G, Balsamo G, Bartlett P, Boike J, Boone A, Chéruy
651 F, Colin J, Cuntz M, Dai Y, Decharme B, Derry J, Ducharme A, Dutra
652 E, Fang X, Fierz C, Ghettas J, Gusev Y, Haverd V, Kontu A, Lafaysse
653 M, Law R, Lawrence D, Li W, Marke T, Marks D, Ménégoz M, Nasonova
654 O, Nitta T, Niwano M, Pomeroy J, Raleigh MS, Schaeffer G, Semenov
655 V, Smirnova TG, Stacke T, Strasser U, Svensson S, Turkov D, Wang T,
656 Wever N, Yuan H, Zhou W, Zhu D (2018) ESM-SnowMIP: Assessing snow
657 models and quantifying snow-related climate feedbacks. *Geoscientific Model
658 Development* 11(12):5027–5049, DOI 10.5194/gmd-11-5027-2018
- 659 Laloyaux P, de Boisseson E, Balmaseda M, Bidlot JR, Broennimann S, Buizza
660 R, Dalhagren P, Dee D, Haimberger L, Hersbach H, Kosaka Y, Martin M,
661 Poli P, Rayner N, Rustemeier E, Schepers D (2018) CERA-20C: A Cou-
662 pled Reanalysis of the Twentieth Century. *Journal of Advances in Modeling
663 Earth Systems* 10(5):1172–1195, DOI 10.1029/2018MS001273
- 664 Landrum L, Otto-Btiesner BL, Wahl ER, Conley A, Lawrence PJ, Rosenbloom
665 N, Teng H (2013) Last millennium climate and its variability in CCSM4.
666 *Journal of Climate* 26(4):1085–1111, DOI 10.1175/JCLI-D-11-00326.1, URL
667 <http://journals.ametsoc.org/doi/abs/10.1175/JCLI-D-11-00326.1>
- 668 Li D, Wrzesien ML, Durand M, Adam J, Lettenmaier DP (2017) How much
669 runoff originates as snow in the western United States, and how will that
670 change in the future? *Geophysical Research Letters* 44(12):6163–6172, DOI
671 10.1002/2017GL073551
- 672 Livezey RE, Smith TM (1999) Considerations for use of the Barnett and
673 Preisendorfer (1987) algorithm for canonical correlation analysis of cli-
674 mate variations. *Journal of Climate* 12(1):303–305, DOI 10.1175/1520-0442-
675 12.1.303
- 676 Malevich SB, Woodhouse CA (2017) Pacific sea surface temperatures, mid-
677 latitude atmospheric circulation, and widespread interannual anomalies in
678 western U.S. streamflow. *Geophysical Research Letters* 44(10):5123–5132,
679 DOI 10.1002/2017GL073536

- 680 Mankin JS, Diffenbaugh NS (2015) Influence of temperature and precipitation
681 variability on near-term snow trends. *Climate Dynamics* 45(3-4):1099–1116,
682 DOI 10.1007/s00382-014-2357-4, URL <http://dx.doi.org/10.1007/s00382-014-2357-4>
- 683 Maraun D, Widmann M (2015) The representation of location by a regional
684 climate model in complex terrain. *Hydrology and Earth System Sciences*
685 19(8):3449–3456, DOI 10.5194/hess-19-3449-2015
- 686 Maraun D, Widmann M (2018) Statistical downscaling and bias correction for
687 climate research. Cambridge University Press
- 688 Marks D, Dozier J (1992) Climate and energy exchange at the snow surface
689 in the Alpine Region of the Sierra Nevada: 2. Snow cover energy balance.
690 *Water Resources Research* 28(11):3043–3054, DOI 10.1029/92WR01483
- 691 Marshall AM, Abatzoglou JT, Link TE, Tennant CJ (2019) Projected Changes
692 in Interannual Variability of Peak Snowpack Amount and Timing in the
693 Western United States. *Geophysical Research Letters* 46(15):8882–8892,
694 DOI 10.1029/2019GL083770
- 695 Maurer GE, Bowling DR (2014) Seasonal snowpack characteristics influence
696 soil temperature and water content at multiple scales in interior western
697 U.S. mountain ecosystems. *Water Resources Research* 50:5375–5377, DOI
698 10.1002/2013WR014452
- 699 McCabe GJ, Dettinger MD (2002) Primary modes and predictability of year-
700 to-year snowpack variations in the Western United States from teleconnec-
701 tions with Pacific Ocean climate. *Journal of Hydrometeorology* 3(1):13–25,
702 DOI 10.1175/1525-7541(2002)003<0013:PMAPOY>2.0.CO;2
- 703 McCabe GJ, Wolock DM (2009) Recent declines in western U.S. snowpack
704 in the context of twentieth-century climate variability. *Earth Interactions*
705 13(12), DOI 10.1175/2009EI283.1
- 706 McCabe GJ, Betancourt JL, Pederson GT, Schwartz MD (2013) Variability
707 common to first leaf dates and snowpack in the western conterminous United
708 States. *Earth Interactions* 17(26):1–18, DOI 10.1175/2013EI000549.1
- 709 McGinnis DL (1997) Estimating climate-change impacts on colorado plateau
710 snowpack using downscaling methods. *Professional Geographer* 49(1):117–
711 125, DOI 10.1111/0033-0124.00062
- 712 Meromy L, Molotch NP, Link TE, Fassnacht SR, Rice R (2013) Subgrid vari-
713 ability of snow water equivalent at operational snow stations in the western
714 USA. *Hydrological Processes* 27(17):2383–2400, DOI 10.1002/hyp.9355
- 715 Mote PW (2003) Trends in snow water equivalent in the Pacific Northwest
716 and their climatic causes. *Geophysical Research Letters* 30(12):1–4, DOI
717 10.1029/2003GL017258
- 718 Mote PW, Li S, Lettenmaier DP, Xiao M, Engel R (2018) Dramatic declines in
719 snowpack in the western US. *npj Climate and Atmospheric Science* 1(1):1–
720 6, DOI 10.1038/s41612-018-0012-1, URL <http://dx.doi.org/10.1038/s41612-018-0012-1>
- 721 Nicholson C, Minckley TA, Shinker JJ (2019) Validating CCSM3 paleoclimate
722 data using pollen-based reconstruction in the intermountain west. *Qua-
723 ternary Science Reviews* 222:105,911, DOI 10.1016/j.quascirev.2019.105911,
- 724
- 725

- 726 URL <https://doi.org/10.1016/j.quascirev.2019.105911>
- 727 North GR, Bell TL, Cahalan RF (1982) Sampling Errors in the Estimation of
728 Empirical Orthogonal Functions
- 729 Otto-Bliesner BL, Brady EC, Fasullo J, Jahn A, Landrum L, Stevenson S,
730 Rosenbloom N, Mai A, Strand G (2016) Climate variability and change
731 since 850 C.E.: An ensemble approach with the Community Earth System
732 Model. *Bulletin of the American Meteorological Society* 97(5):787–801, DOI
733 10.1175/BAMS-D-14-00233.1
- 734 Pederson GT, Gray ST, Woodhouse CA, Betancourt JL, Fagre DB, Littell
735 JS, Watson E, Luckman BH, Graumlich LJ (2011) The Unusual Nature
736 of Recent Snowpack Declines in the North American Cordillera. *Science*
737 333:332–335, DOI 10.1126/science.1201570
- 738 Pederson GT, Betancourt JL, McCabe GJ (2013) Regional patterns and prox-
739 imal causes of the recent snowpack decline in the Rocky Mountains, U.S.
740 *Geophysical Research Letters* 40(9):1811–1816, DOI 10.1002/grl.50424
- 741 Pierce DW, Barnett TP, Hidalgo HG, Das T, Bonfils C, Santer BD, Bala G,
742 Dettinger MD, Cayan DR, Mirin A, Wood AW, Nozawa T (2008) Attri-
743 bution of declining Western U.S. Snowpack to human effects. *Journal of*
744 *Climate* 21(23):6425–6444, DOI 10.1175/2008JCLI2405.1
- 745 Pons MR, San-Martín D, Herrera S, Gutiérrez JM (2010) Snow trends
746 in Northern Spain: Analysis and simulation with statistical downscaling
747 methods. *International Journal of Climatology* 30(12):1795–1806, DOI
748 10.1002/joc.2016
- 749 Redmond KT, Koch RW (1991) Surface Climate and Streamflow Variabil-
750 ity in the Western United States and Their Relationship to Large-Scale
751 Circulation Indices. *Water Resources Research* 27(9):2381–2399, DOI
752 10.1029/91WR00690
- 753 Reusch DB, Alley RB, Hewitson BC (2005) Relative performance of self-
754 organizing maps and principal component analysis in pattern extraction
755 from synthetic climatological data. *Polar Geography* 29(3):188–212, DOI
756 10.1080/789610199
- 757 Rhoades AM, Ullrich PA, Zarzycki CM (2018) Projecting 21st century snow-
758 pack trends in western USA mountains using variable-resolution CESM.
759 *Climate Dynamics* 50(1-2):261–288, DOI 10.1007/s00382-017-3606-0
- 760 Richman MB (1986) Review Article: Rotation of principal components. *Jour-
761 nal of Climatology* 6(March):293–335, DOI 10.1056/NEJMra1313875
- 762 Rutter N, Essery R, Pomeroy J, Altimir N, Andreadis K, Baker I, Barr A,
763 Bartlett P, Boone A, Deng H, Douville H, Dutra E, Elder K, Ellis C, Feng X,
764 Gelfan A, Goodbody A, Gusev Y, Gustafsson D, Hellström R, Hirabayashi
765 Y, Hirota T, Jonas T, Koren V, Kuragina A, Lettenmaier D, Li WP, Luce C,
766 Martin E, Nasonova O, Pumpanen J, Pyles RD, Samuelsson P, Sandells M,
767 Schädler G, Shmakin A, Smirnova TG, Stähli M, Stöckli R, Strasser U, Su H,
768 Suzuki K, Takata K, Tanaka K, Thompson E, Vesala T, Viterbo P, Wiltshire
769 A, Xia K, Xue Y, Yamazaki T (2009) Evaluation of forest snow processes
770 models (SnowMIP2). *Journal of Geophysical Research Atmospheres* 114(6),
771 DOI 10.1029/2008JD011063

- 772 Schoenemann SW, Martin JT, Pederson GT, McWethy DB (2020) 2,200-Year
773 tree-ring and lake-sediment based snowpack reconstruction for the northern
774 Rocky Mountains highlights the historic magnitude of recent snow drought.
775 Quaternary Science Advances 2:100,013, DOI 10.1016/j.qsa.2020.100013
- 776 Seager R, Kushnir Y, Nakamura J, Ting M, Naik N (2010) Northern Hemi-
777 sphere winter snow anomalies: ENSO, NAO and the winter of 2009/10.
778 Geophysical Research Letters 37(14), DOI 10.1029/2010GL043830
- 779 Serreze MC, Clark MP, Armstrong RL, McGinnis DA, Pulwarty RS (1999)
780 Characteristics of the western United States snowpack from snowpack
781 telemetry (SNOWTEL) data. Water Resources Research 35(7):2145–2160,
782 DOI 10.1029/1999WR900090
- 783 Siler N, Proistosescu C, Po-Chedley S (2019) Natural Variability Has
784 Slowed the Decline in Western U.S. Snowpack Since the 1980s. Geophys-
785 ical Research Letters 46(1):346–355, DOI 10.1029/2018GL081080, URL
786 <http://doi.wiley.com/10.1029/2018GL081080>
- 787 Simon T, Hense A, Su B, Jiang T, Simmer C, Ohlwein C (2013) Pattern-
788 based statistical downscaling of East Asian summer monsoon precipitation.
789 Tellus, Series A: Dynamic Meteorology and Oceanography 65:1–12, DOI
790 10.3402/tellusa.v65i0.19749
- 791 Smerdon JE, Kaplan A, Chang D, Evans MN (2010) A pseudoproxy
792 evaluation of the CCA and RegEM methods for reconstructing climate
793 fields of the last millennium. Journal of Climate 23(18):4856–4880, DOI
794 10.1175/2010JCLI3328.1
- 795 Tennant CJ, Harpold AA, Lohse KA, Godsey SE, Crosby BT, Larsen LG,
796 Brooks PD, Van Kirk RW, Glenn NF (2017) Regional sensitivities of
797 seasonal snowpack to elevation, aspect, and vegetation cover in west-
798 ern North America. Water Resources Research 53(8):6908–6926, DOI
799 10.1002/2016WR019374
- 800 Tippett MK, DelSole T, Mason SJ, Barnston AG (2008) Regression-based
801 methods for finding coupled patterns. Journal of Climate 21(17):4384–4398,
802 DOI 10.1175/2008JCLI2150.1
- 803 Towler E, PaiMazumder D, Holland G (2017) A framework for investigating
804 large-scale patterns as an alternative to precipitation for downscaling to local
805 drought. Climate Dynamics 48:881–892, DOI 10.1007/s00382-016-3116-5
- 806 Tryhorn L, Degaetano A (2013) A methodology for statistically downscaling
807 seasonal snow cover characteristics over the Northeastern United States. In-
808 ternational Journal of Climatology 33(12):2728–2743, DOI 10.1002/joc.3626
- 809 Van Den Dool HM (1987) A Bias in Skill in Forecasts Based on Analogues
810 and Antilogues. Journal of Climate and Applied Meteorology 26:1278–1281
- 811 Wainer J, Cawley G (2018) Nested cross-validation when selecting classifiers
812 is overzealous for most practical applications. arXiv preprint pp 1–9, URL
813 <http://arxiv.org/abs/1809.09446>, 1809.09446
- 814 Walsh JE, Tucek DR, Peterson MR (1982) Seasonal Snow Cover and Short-
815 Term Climatic Fluctuations over the United States. Monthly Weather Re-
816 view 110(10):1474—1486

- 817 Wickham H, Averick M, Bryan J, Chang W, McGowan L, François R, Grole-
818 mund G, Hayes A, Henry L, Hester J, Kuhn M, Pedersen T, Miller E, Bache-
819 S, Müller K, Ooms J, Robinson D, Seidel D, Spinu V, Takahashi K, Vaughan
820 D, Wilke C, Woo K, Yutani H (2019) Welcome to the Tidyverse. *Journal of*
821 *Open Source Software* 4(43):1686, DOI 10.21105/joss.01686
- 822 Wilks DS (2006) On "field significance" and the false discovery rate. *Jour-*
823 *nal of Applied Meteorology and Climatology* 45(9):1181–1189, DOI
824 10.1175/JAM2404.1
- 825 Wilks DS (2014) Probabilistic canonical correlation analysis forecasts, with ap-
826 plication to tropical Pacific sea-surface temperatures. *International Journal*
827 *of Climatology* 34(5):1405–1413, DOI 10.1002/joc.3771
- 828 Wilks DS (2016) "The stippling shows statistically significant grid points":
829 How research results are routinely overstated and overinterpreted, and what
830 to do about it. *Bulletin of the American Meteorological Society* 97(12):2263–
831 2273, DOI 10.1175/BAMS-D-15-00267.1
- 832 Wood SN (2006) Generalized Additive Models: An Introduction with R. Chap-
833 man and Hall/CRC press, DOI 10.1111/j.1541-0420.2006.00574.x, URL
834 <http://opus.bath.ac.uk/7011/>
- 835 Woodhouse CA (2003) A 431-Yr Reconstruction of Western Colorado
836 Snowpack from Tree Rings. *Journal of Climate* 16(10):1551–1561, DOI
837 10.2307/26249719
- 838 Xiao M, Udall B, Lettenmaier DP (2018) On the Causes of Declining Col-
839 orado River Streamflows. *Water Resources Research* 54(9):6739–6756, DOI
840 10.1029/2018WR023153
- 841 Xu Y, Jones A, Rhoades A (2019) A quantitative method to decompose SWE
842 differences between regional climate models and reanalysis datasets. *Scienc-*
843 *tific Reports* 9(1):1–11, DOI 10.1038/s41598-019-52880-5
- 844 Ye K (2019) Interannual variability of March snow mass over North-
845 ern Eurasia and its relation to the concurrent and preceding sur-
846 face air temperature, precipitation and atmospheric circulation. *Cli-*
847 *mate Dynamics* 52(5-6):2813–2836, DOI 10.1007/s00382-018-4297-x, URL
848 <http://dx.doi.org/10.1007/s00382-018-4297-x>
- 849 Zeng X, Broxton P, Dawson N (2018) Snowpack Change From 1982 to
850 2016 Over Conterminous United States. *Geophysical Research Letters*
851 45(23):12,940–12,947, DOI 10.1029/2018GL079621